Adaptive Duty Cycling in Sensor Networks with Energy Harvesting using Continuous-Time Markov Chain and Fluid Models

Wai Hong Ronald Chan*, Pengfei Zhang†, Ido Nevat†, Sai Ganesh Nagarajan†,
Alvin Valera‡, Hwee-Xian Tan‡ and Natarajan Gautam§
*Mechanical Engineering, Stanford University, California, United States †Institute for Infocomm Research (I^{2}R), Singapore ‡School of Information Systems, Singapore Management University (SMU), Singapore
§Industrial and Systems Engineering, Texas A&M University, Texas, United States

***Abstract*—The dynamic and unpredictable nature of energy harvesting sources available for wireless sensor networks, and the time variation in network statistics like packet transmission rates and link qualities, necessitate the use of adaptive duty cycling techniques. Such adaptive control allows sensor nodes to achieve long-run energy neutrality, where energy supply and demand are balanced in a dynamic environment such that the nodes function continuously.**

In this paper, we develop a new framework enabling an adaptive duty cycling scheme for sensor networks that takes into account the node battery level, ambient energy that can be harvested, and application-level QoS requirements. We model the system as a Markov Decision Process (MDP) that modifies its state transition policy using reinforcement learning. The MDP uses Continuous Time Markov Chains (CTMCs) to model the network state of a node in order to obtain key QoS metrics like latency, loss probability and power consumption, as well as to model the node battery level taking into account physically feasible rates of change. We show that with an appropriate choice of the reward function for the MDP, as well as a suitable learning rate, exploitation probability and discount factor, the need to maintain minimum QoS levels for optimal network performance can be balanced with the need to promote the maintenance of a finite battery level to ensure node operability. Extensive simulation results show the benefit of our algorithm for different reward functions and parameters.

I. Introduction

Wireless sensor networks (WSNs) can be used in a large number of applications, such as environmental and structural health monitoring, weather forecasting [1]–[3], surveillance, health care, and home automation [4]. A key challenge that constrains the operation of sensor networks is limited lifetime arising from the finite energy storage in each node [5]. However, recent advances in energy harvesting technologies are enabling the deployment of sensor nodes that are equipped with a replenishable supply of energy [6]–[10]. These techniques can potentially eliminate the limited lifetime problem in sensor networks and enable perpetual operation without the need for battery replacement, which is not only labourious and expensive, but also infeasible in certain situations.

Despite this, the uninterrupted operation of energy harvesting-powered wireless sensor networks (EH-WSNs) remains a major challenge, due to the unpredictable and dynamic nature of the harvestable energy supply [5], [11].

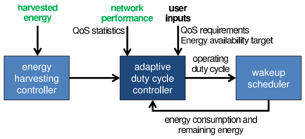
harvested energy
network performance
user inputs
QoS statistics
QoS requirements
Energy availability target
energy harvesting controller
adaptive duty cycle controller
operating duty cycle
wakeup scheduler
energy consumption and remaining energy

Fig. 1. Main components of proposed adaptive scheme. Quantities that fluctuate due to environmental influences are marked in green.

To cope with the energy supply dynamics, adaptive duty cycling techniques [11]–[17] have been proposed. The common underlying objective of these techniques is to attain an optimal *energy-neutral* point at every node, wherein the energy supply and energy demand are balanced. Also, other works focus on optimizing energy consumption in EH-WSNs by formulating the response to a time-varying harvesting profile as a Markov Decision Process (MDP) or other probability-driven processes [18], [19]. These energy-oriented techniques tend to focus primarily on obtaining the optimal per-node duty cycle to prolong network lifetime, while neglecting application-level quality of service (QoS) requirements [20]–[22]. More recently, adaptive duty cycling techniques involving MDPs have been proposed that focus on achieving energy efficient operations while considering a subset of the QoS requirements (such as throughput or delay) with full channel state information [23]–[27], but without considering the long-term energy availability of the system or tolerating ambiguity in the state information.

In this paper, we develop a novel framework enabling an adaptive duty cycling scheme that allows network designers to trade-off between both short-term QoS requirements and long-term energy availability using an adaptive reinforcement learning algorithm. In our framework, the QoS metrics of the system are estimated based on knowledge of the average performance of the network, such as the average packet transmission and probing rates, without necessarily requiring knowledge of the full channel state information. These quantities can be monitored online or estimated offline with a time delay depending on the requirements of the system. Fig. 1 illustrates the main components of such a scheme, which comprises the following: (i) energy harvesting controller; (ii) adaptive duty cycle controller; and (iii) wakeup scheduler.

The energy harvesting controller provides information on the amount of harvested energy that is currently available, while predicting the harvested energy available within the next few hours, depending on the diurnal cycles of the energy sources. The adaptive duty cycle controller computes the optimal operating duty cycle based on user inputs (in the form of application QoS requirements) and the available amount of harvested energy. The wakeup scheduler will then: (i) manage the sleep and wake interfaces of each node, based on the recommended operating duty cycle, and (ii) provide feedback to the adaptive duty cycle controller on the energy consumption of and remaining energy in the node. This feedback loop allows the duty cycle controller to **adapt** its duty cycle, based on the harvested and remaining energies - in order to meet QoS requirements - via operating policies such as energy neutrality.

In our previous work [28], we developed a duty cycle controller key to the energy-aware operations of a sensor network. Using a Continuous Time Markov Chain (CTMC) model, we derived key QoS metrics including *loss probability*, *latency*, as well as *power consumption*, as functions of the duty cycle. (We define these metrics more explicitly in Section III-B.) We then formulated and solved the optimal operating duty cycle as a non-linear optimization problem, using latency and loss probability as the constraints. We validated our CTMC model through Monte Carlo simulations and demonstrated that a Markovian duty cycling scheme can outperform periodic duty cycling schemes. In this paper, we extend the previous work and enhance the duty cycle controller by considering the battery level and energy harvesting rate. We then formulate the adaptive duty cycle problem as a MDP model. The states of the MDP model correspond to the energy consumption rates at which the node can operate. The actions refer to the transition rates between the various duty cycle values that the node can adopt. The reward function is derived based on the QoS parameters derived in the previous paper, as well as on the energy availability of the battery based on a fluid model [29]–[31] that indicates the ability of the node to function continuously. While finding the optimal duty cycle scheme to operate under is a nonconvex optimization problem which is hard to implement on-line, we propose a relatively simple on-line approach which uses reinforcement learning [32], [33] to heuristically update the reward function to approximate convergence. We also use extensive simulations to show that the MDP converges to a desirable result quickly, and to compare our approach with a random approach to demonstrate the performance of the MDP scheme.

In this work, we make several key contributions: (i) we enable a WSN to determine its duty cycle control through simultaneous consideration of the energy supply dynamics and application-level QoS requirements; (ii) we establish a reward framework that allows the network to tune the relative importance of the energy availability and the QoS requirements; (iii) we implement a reinforcement learning algorithm that converges to a desirable solution quickly and with lower computational complexity than convergence to a fully optimal solution; and (iv) we allow the system to adapt to changes in the environment and/or the network that occur at timescales larger than the convergence time of the learning curve. In Fig. 2, we provide an approximate comparison of the timescales involved in our system.

The rest of the paper is organized as follows. Section II provides details on the key assumptions used in the system model for a battery-free framework. In Section III, we derive network performance metrics using a CTMC model. We extend the system model to incorporate battery levels in Section IV, and describe the behaviour of the battery with another CTMC model in Section V. In Section VI, we allow the system to determine the optimal rates of transition between its constituent states using a MDP model. Simulation results are presented in Section VII. Section VIII concludes the paper.

II. System Model for Battery-Free Framework

In this Section, we develop a probabilistic model that describes the features of a single WSN node, i.e. data reception from other nodes and data transmission towards the gateway (GW) via another node. Both this node and its recipient node are duty cycled, and several QoS parameters are investigated as functions of this duty cycle. Under the framework developed in this Section, we do not consider the role of energy harvesting. Thus, we assume the network is powered by mains electricity, and the effective battery capacity of each node is unlimited (although we would still try to minimise the energy consumption of each node). In Section IV, we will generalise our framework by considering energy harvesting nodes.

We now present all the statistical assumptions of our framework and provide details of various system components required, such as the traffic model, channel model and packet transmission schemes. The notation used in this section is shown in Table I.

1) Node State: Each node v_j is in one of the following states $N_j \in \{0,1\}$ at any point in time, where $N_j = 0$ and $N_j = 1$ denote that v_j is in the *asleep* and *awake* states respectively. The duration t that node v_j is in each of the states N_j is a random variable that follows an exponential distribution:
$$p(t) = \begin{cases} \gamma_i \cdot e^{-\gamma_i \cdot t} & t \geq 0 \\ 0 & t < 0, \end{cases} \tag{1}$$
where γ_i, $i \in \{0,1\}$ are the rates of the asleep and awake states. The average long-term fraction of time that the node is *awake* is given by $q = \frac{1}{\gamma_1 \cdot T}$ where $T = \frac{1}{\gamma_0} + \frac{1}{\gamma_1}$ is the average cycle time.
2) Traffic Model: The number of data packets d_0 generated by each node follows a Poisson distribution with an average rate of λ_0 packets per unit time, i.e., $d_0 \sim \text{Pois}(\lambda_0)$. In addition, the node receives d_n packets from all of its neighbours according to a Poisson process $d_n \sim \text{Pois}(\lambda)$.
3) Wireless Channel Model: The time-varying wireless link quality is modelled by the classical Gilbert-Elliot Markovian model [34], [35] with two states $L \in \{0,1\}$, where $L = 0$ and $L = 1$ denote that the channel quality is *bad* and *good* respectively. The duration t that a node is

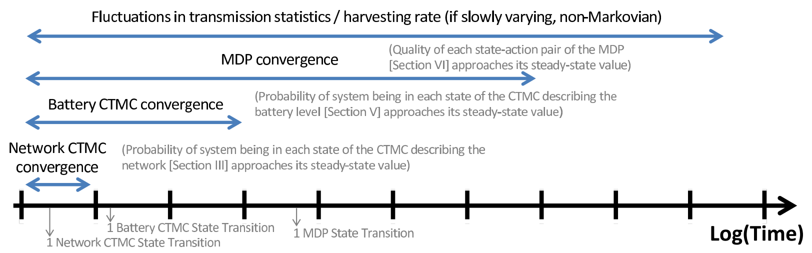
Fluctuations in transmission statistics / harvesting rate (if slowly varying, non-Markovian)
MDP convergence
(Quality of each state-action pair of the MDP [Section VI] approaches its steady-state value)
Battery CTMC convergence
(Probability of system being in each state of the CTMC describing the battery level [Section V] approaches its steady-state value)
Network CTMC convergence
(Probability of system being in each state of the CTMC describing the network [Section III] approaches its steady-state value)
1 Battery CTMC State Transition
1 Network CTMC State Transition
1 MDP State Transition
Log(Time)

Fig. 2. Comparison of timescales involved in our system.

TABLE I
NOTATION USED IN SECTION II

Notation	Description	Value
v_j	j-th node	N.A.
v_k	Downstream node	N.A.
N_j	$Awake$ or $Asleep$ states of v_j	$\{0, 1\}$
γ_i	Respective rates of asleep ($N_j = i = 0$) / awake ($N_j = i = 1$) states	$\mathbb{R}^+$
T	Average cycle time	$\frac{1}{\gamma_0} + \frac{1}{\gamma_1}$
q	Average long-term fraction of time in which node is in the $awake$ state	$\frac{1}{\gamma_1 T}$
λ_0	Average self-packet generation rate	$\mathbb{R}^+$
λ	Average received-packet rate from nearby nodes	$\mathbb{R}^+$
d_0	Number of self-packets generated by each node	d_0 ~Pois(λ_0)
d_n	Number of received-packets from nearby nodes	d_n ~Pois(λ)
L	Wireless link quality	$\{0, 1\}$
c_i	Average rate of *bad* ($i = 0$) and *good* ($i = 1$) link quality states	$\mathbb{R}^+$
β	Probabilities of successfully delivered data packets when channel is in *bad* link quality state	[0,1]
α	Probabilities of successfully delivered data packets when channel is in *good* link quality state	[0,1]
θ_g	Intensities of probing when channel is good	$\mathbb{R}^+$
θ_b	Intensities of probing when channel is bad	$\mathbb{R}^+$
$\mathcal{X}_n$	No Retransmissions	N.A.
$\mathcal{X}_r$	Retransmissions	N.A.
λ_g	Average number of successfully received packets at a node under good channel conditions	$\mathbb{R}^+$
λ_b	Average number of successfully received packets at a node under bad channel conditions	$\mathbb{R}^+$
$\mathcal{P}_{asleep}$	Power consumption of a node in the asleep state	$\mathbb{R}^+$
$\mathcal{P}_{awake}$	Power consumption of a node in the awake state	$\mathbb{R}^+$
$\mathcal{P}_{probe}$	Power consumption of probing mechanism	$\mathbb{R}^+$
ε_{tx}	Energy consumed to transmit a single data packet	$\mathbb{R}^+$

in each of the channel states is a random variable that follows an exponential distribution:

$$p(t) = \begin{cases} c_i \cdot e^{-c_i \cdot t} & t \geq 0 \\ 0 & t < 0, \end{cases} \tag{2}$$

where c_i, $i \in \{0, 1\}$ are the respective rates of the *bad* and *good* states. We let β and α denote the probabilities of successfully delivered data packets when the channel is in the *bad* and *good* states respectively. Acknowledgment packets are assumed to always be delivered successfully.

4) Probing Mechanism: The network utilizes probes to determine if an arbitrary downstream node v_k is in an awake state $N_k = 1$, prior to the commencement of data transmission. The probing mechanism is modelled as a Poisson process, with intensities θ_g and θ_b when the channel quality is good and bad respectively. The reception of a probe-acknowledgment by the transmitter node v_j indicates that v_k is awake; v_j will then instantaneously transmit *all* its data packets to v_k.

5) Transmission Schemes: We consider two transmission schemes:

a) **No Retransmissions**: data packets that have not been successfully delivered to the receiver (due to poor channel quality) will **not** be retransmitted. The corresponding average numbers of packets that successfully arrive at a node under good and poor channel conditions are denoted as λ_g and λ_b respectively, where $\lambda_b = \frac{\beta \cdot \lambda_g}{\alpha}$. We denote this scheme by $\mathcal{X}_n$.

b) **Retransmissions**: data packets are retransmitted until they are successfully delivered to the receiver. The corresponding average number of packets that successfully arrive under this scheme is λ, where $\lambda_g = \lambda_b = \lambda$. The effective packet arrival rate when the node is in the awake state is $\frac{\lambda}{q}$. We denote this scheme by $\mathcal{X}_r$.

6) Power Consumption Parameters: The power consumptions of a node in the asleep and awake states are $\mathcal{P}_{asleep}$ and $\mathcal{P}_{awake}$ respectively. The power consumption of the probing mechanisms is denoted as $\mathcal{P}_{probe}$. The energy incurred to transmit a single data packet is $\mathcal{E}_{tx}$.

With these definitions, we now present in the next Section a probabilistic model based on a Continuous Time Markov Chain (CTMC) model, and derive the QoS parameters of interest.

III. CTMC Model For Node Performance State (Battery-Free; Fixed Duty Cycle)

In this Section, we design a probabilistic model to describe the performance of a single node in the WSN for a fixed duty cycle q. To this end, we model the system as a CTMC, as shown in Fig. 3. In addition, we assume that the system evolves independently of the battery level, as we will be using this model to generate instantaneous QoS metrics for the system, assuming in addition that the timescale of energy fluctuations exceeds the timescale of packet traffic equilibration (i.e. the convergence time of this CTMC). The notation used in this section is shown in Table II.

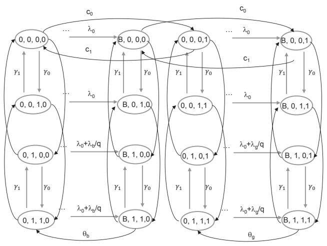

Fig. 3. CTMC model of a two-node section of a network. The CTMC is guided by the transition rate matrix $\mathcal{Q}$.

A. CTMC State Space Model

We consider a 4-tuple CTMC state space as follows:

1) Node buffer: Each node has a FIFO buffer of finite size B. The number of packets in the finite queue is denoted by $b \in \{0, 1, \ldots, B\}$.
2) Node state: As mentioned in Section II, each node v_j is in state $N_j \in \{0, 1\}$ at any one time, depending on whether it is *asleep* ($N_j = 0$) or *awake* ($N_j = 1$).
3) Downstream node state: An arbitrary downstream (receiving) node v_k is in state $N_k \in \{0, 1\}$ at any one time, depending on whether it is *asleep* ($N_k = 0$) or *awake* ($N_k = 1$).
4) Link quality: The wireless link quality is in state $L \in \{0, 1\}$ at any one time, depending on whether the channel is *bad* ($L = 0$) or *good* ($L = 1$). (We note that it is straightforward to extend the analysis to multiple link quality states.)

Given these definitions, the state space $\mathcal{S}$ can be written as the following Cartesian product $\mathcal{S} = \{0, 1, \ldots, B\} \times \{0, 1\} \times \{0, 1\} \times \{0, 1\} \in \mathcal{R}^{|b| \times |N_j| \times |N_k| \times |L|}$. The corresponding cardinality of the state space is given by $|\mathcal{S}| = 8(B + 1)$.

B. QoS metric definitions

We now present the following key QoS metrics of interest:

- *loss probability* due to wireless channel transmission errors and packet drops arising from buffer overflows, denoted $\pi\left(q\right)$;
- *latency* incurred by holding packets in the transmission queue, denoted $\ell\left(q\right)$;
- and *average power consumption* incurred by a node, denoted $\rho\left(q\right)$.

In the next Lemma we present the derived expressions for these QoS metrics for the two cases under consideration, namely the Retransmissions and No Retransmissions schemes.

Lemma 1. ***QoS metrics under Retransmissions scheme*** *The QoS parameters are given by (5).*

Proof. See Appendix A. □

Lemma 2. ***QoS metrics under No Retransmissions scheme*** *The QoS parameters are given by (6).*

Proof. See Appendix B. □

By defining parameters (e.g. packet arrival rates λ_0 and λ, probing intensities θ_g and θ_b, and maximum buffer size B) of the transitive matrix $\mathcal{Q}$ according to parameters of the actual sensor network, we can obtain the optimal duty cycle q in terms of the asleep and awake rates γ_0 and γ_1. This is presented next.

C. Optimal Duty Cycle

To find the optimal duty cycle, different criteria can be considered. Here, we choose to find the duty cycle which minimizes the power consumption, while satisfying application-level QoS constraints. We note that other criteria could be considered and our framework is general enough to handle them as well.

For our criterion, the resulting optimisation problem is given as follows:

$$q = \arg\min_{q} \rho(q) \qquad \text{subject to} \quad \pi(q) \leq \pi_0, \ell(q) \leq \ell_0, q \geq 0 \tag{3}$$

where π_0 and ℓ_0 are pre-defined latency and loss thresholds.

Recall that γ_1 and γ_0 can be expressed as functions of q and the average cycle time T as follows:

$$\gamma_1 = \frac{1}{T \cdot q} \qquad\qquad \gamma_0 = \frac{1}{T \cdot (1 - q)} \tag{4}$$

Thus, we can further simplify the optimisation problem to a single parameter optimization problem by defining T and solving for γ_1 and γ_0. Hence, even though the optimization problem in (3) does not have an analytical closed form expression, it is easy to find the optimal q (denoted q^*) numerically via simple evaluation on a finely divided grid. In Fig. 4, we plot the optimal duty cycle of the system after constraint optimization for various latency and loss probability constraints, as well as for different sets of system parameters. Note that there are regions in which the constraints cannot be satisfied simultaneously.

IV. System Model for Framework with Finite Battery Level and Energy Harvesting

In this Section and the next, we develop a framework that describes the evolution of the battery level of a single

TABLE II
NOTATION USED IN SECTION III

Notation	Description	Value
B	FIFO buffer size	$\mathbb{Z}^+$
b	Number of packets in finite queue	$b \in \{0, 1, \cdots, B\}$
N_k	*Awake* or *Asleep* states of v_k	$\{0, 1\}$
$\mathcal{S}$	State space	$\{0, 1, \cdots, B\} \times \{0, 1\} \times \{0, 1\} \times \{0, 1\}$
s_k	Arbitrary state	$s_k \in \mathcal{S}$
p_k	Steady-state probability of state s_k	$(0, 1)$
$\mathcal{Q}$	Transition matrix of CTMC for node performance states	N.A.
$\pi(q)$	Loss probability	$[0, 1]$
$\bar{b}$	Average number of packets in the buffer	$\mathbb{R}^+$
λ_e	Effective packet arrival rate at the node	$\mathbb{R}^+$
$\ell(q)$	Latency	$\ell = \frac{b}{\lambda_e}$
$\rho(q)$	Average power consumption of node v_j	$\mathbb{R}^+$

$$\begin{aligned}
\pi\left(q\right) &= \sum_{k=0}^{1} \frac{p_{B,1,0,k}(\lambda/q+\lambda_0)}{\lambda/q+\lambda_0+\gamma_0+\gamma_1+c_k} + \sum_{k=0}^{1} \frac{p_{B,1,1,k}(\lambda/q+\lambda_0)}{\lambda/q+\lambda_0+2\gamma_1+\theta+c_k} + \sum_{k=0}^{1} \frac{p_{B,0,0,k}\lambda_0}{\lambda_0+2\gamma_0+c_k} + \sum_{k=0}^{1} \frac{p_{B,0,1,k}\lambda_0}{\lambda_0+\gamma_0+\gamma_1+c_k} \\
\ell\left(q\right) &= \frac{1}{\lambda+\lambda_0} \sum_{b=0}^{B}\sum_{i=0}^{1}\sum_{j=0}^{1}\sum_{k=0}^{1} b p_{b,i,j,k} \qquad (5) \\
\rho\left(q\right) &= \mathcal{P}_{asleep} \sum_{b=0}^{B}\sum_{j=0}^{1}\sum_{k=0}^{1} p_{b,0,j,k} + \mathcal{P}_{awake} \sum_{b=0}^{B}\sum_{j=0}^{1}\sum_{k=0}^{1} p_{b,1,j,k} + \mathcal{P}_{probe} \sum_{b=1}^{B}\sum_{j=0}^{1}\sum_{k=0}^{1} p_{b,1,j,k} + \left(\frac{\lambda}{1-\beta/\alpha}+\lambda_0\right)\mathcal{E}_{tx}
\end{aligned}$$

$$\begin{aligned}
\pi\left(q\right) = &\frac{p_{B,1,0,0}(\lambda_b/q+\lambda_0)}{\lambda_b/q+\lambda_0+\gamma_0+\gamma_1+c_0} + \frac{p_{B,1,1,0}(\lambda_b/q+\lambda_0)}{\lambda_b/q+\lambda_0+2\gamma_1+\theta+c_0} + \frac{p_{B,0,0,0}\lambda_0}{\lambda_0+2\gamma_0+c_0} + \frac{p_{B,0,1,0}\lambda_0}{\lambda_0+\gamma_0+\gamma_1+c_0} + \\
&\frac{p_{B,1,0,1}(\lambda_g/q+\lambda_0)}{\lambda_g/q+\lambda_0+\gamma_0+\gamma_1+c_1} + \frac{p_{B,1,1,1}(\lambda_g/q+\lambda_0)}{\lambda_g/q+\lambda_0+2\gamma_0+\gamma_1+c_1} + \frac{p_{B,0,0,1}\lambda_0}{\lambda_0+2\gamma_0+c_1} + \frac{p_{B,0,1,1}\lambda_0}{\lambda_0+\gamma_0+\gamma_1+c_1} \\
\ell\left(q\right) = &\frac{1}{\lambda_b+\lambda_0} \sum_{b=0}^{B}\sum_{i=0}^{1}\sum_{j=0}^{1} b p_{b,i,j,0} + \frac{1}{\lambda_g+\lambda_0} \sum_{b=0}^{B}\sum_{i=0}^{1}\sum_{j=0}^{1} b p_{b,i,j,1} \qquad (6) \\
\rho\left(q\right) = &\mathcal{P}_{asleep} \sum_{b=0}^{B}\sum_{j=0}^{1}\sum_{k=0}^{1} p_{b,0,j,k} + \mathcal{P}_{awake} \sum_{b=0}^{B}\sum_{j=0}^{1}\sum_{k=0}^{1} p_{b,1,j,k} + \mathcal{P}_{probe} \sum_{b=1}^{B}\sum_{j=0}^{1}\sum_{k=0}^{1} p_{b,1,j,k} + (\lambda+\lambda_0)\mathcal{E}_{tx}
\end{aligned}$$

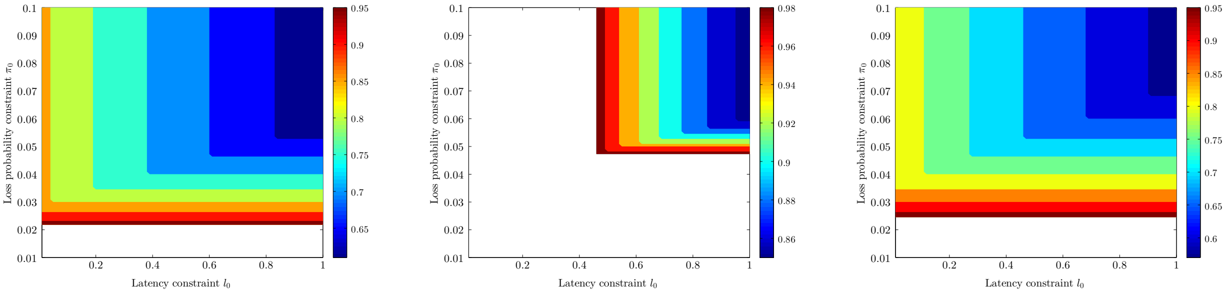

(a) (b) (c)

Fig. 4. Optimal duty cycle as a function of the QoS constraints for different sets of system parameters. The optimal duty cycle is represented by a colour whose corresponding value can be read off from the colour bar. Steps are observed because the duty cycle was sampled discretely.

node with finite battery capacity and the capability to harvest energy from the environment. Under the constraints of this framework, we eventually identify a set of variables that can be designed to control the performance of the network, namely the transition rates that govern the transition of the battery state between different rates of energy harvesting and consumption. The consumption rates were previously derived in Section III. Note that the battery states in this Section and the next are distinct from the CTMC states of Sections II and III, which describe the network status and capacity of the node.

Here, we provide details of additional system components required in this framework, in particular the battery model and its time evolution. The notation used in this section is shown in Table III.

1) Battery Model: The battery level $X(t)$ of the sensor node is treated in a continuous fashion, i.e. $X(t) \in \mathcal{R}$ and $X(t) \in [0, C]$, where C is the capacity of the battery and $t \geq 0$.
2) Rate of Change of Battery Level: In reality, the rate of change of $X(t)$ can take any value in a continuous, bounded interval $[\dot{X}_{\text{min}}, \dot{X}_{\text{max}}]$ where $\dot{X}_{\text{min}}$ and $\dot{X}_{\text{max}}$ are the minimum and maximum possible rates determined by the battery chemistry, the maximum harvesting power available, and the maximum power consumption of the node.

   We model this with a *fluid model* by sampling mn possible rates within this interval, and defining the cardinality of the state space of the battery to be mn. Let $Z(t)$ be the state of the battery at time t. When $Z(t)$ is in some state $i \in T = \{1, 2, \ldots, mn\}$, the evolution of the process satisfies

$$\frac{dX(t)}{dt} = \begin{cases} \max(0, r_i) & \text{if } X(t) = 0, \\ r_i & \text{if } 0 < X(t) < C, \\ \min(0, r_i) & \text{if } X(t) = C, \end{cases} \tag{7}$$

   where r_i is the rate governing the process evolution corresponding to state i provided the battery is neither full nor empty. In this model, if the battery is full, the rate of change of $X(t)$ with respect to time cannot take positive values; if the battery is empty, the rate of change of $X(t)$ with respect to time cannot take negative values. This allows us to model the continuous nature of the battery level using a set of discrete states that best describe the time evolution of the battery level by characterizing the most common rates of change in the battery level.

   Physically, the change in the battery level $X(t)$ is driven by two processes: the harvesting of energy from the surroundings at rate h_k, and the consumption of energy by the system at rate u_l.

   a) Discretized Energy Harvesting Rate: In reality, the energy harvesting rate h_k can take any value between zero and the maximum physically possible harvesting rate h_{max}. We model this by sampling m possible harvesting rates between zero and h_{max}.

   b) Discretized Energy Consumption Rate: In reality, the energy consumption rate u_l can take any value between zero and the maximum physically possible consumption rate u_{max}. We model this by sampling n possible consumption rates between zero and u_{max}. As demonstrated in our previous paper [28], u_l can be modelled as a monotonic function of the duty cycle q.

   c) Discretized Rate of Change of Battery Level: Now, we set $k, l \in \mathcal{Z}$, $k \in (0, m]$ and $l \in (0, n]$, and we define

$$r_{n(k-1)+l} = h_k - u_l, \tag{8}$$

   choosing $\{h_k\}$ and $\{u_l\}$ such that the resulting r_i are unique. Note $\dot{X}_{\text{min}} = -u_{\text{max}}$ and $\dot{X}_{\text{max}} = h_{\text{max}}$.

V. CTMC Model For Node Battery State (Variable Duty Cycle)

With the model described in the previous Section, we can now extend our framework so that it also captures the time evolution of the battery level of a single node in the network. Based on this extended framework, we can thereby describe the *energy availability* of the battery in terms of a probabilistic description of the amount of time the battery level is above zero, as well as a *transition rate matrix* that describes the transition of the system from one set of energy harvesting and consumption rates to another set. By isolating the transitions between different harvesting rates from the transitions between different consumption rates, we then separate the influences of the environment from a potential set of user inputs for system optimization. The notation used in this section is shown in Table IV.

A. Characteristics of CTMC describing transitions between battery states

Here, we introduce a CTMC that describes the transitions between the mn battery states. This allows us to concretely set up the battery model, as well as to generate the energy availability required for the reward function of the Markov decision process (MDP) to be presented in Section VI.

Suppose the CTMC has a generator matrix $\mathcal{Q}_e^{MDP} = [q_{e,ij}]$. Let us define a drift matrix

$$D = \begin{bmatrix} r_1 & & & \\ & r_2 & & \mathbf{0} \\ & & \ddots & \\ \mathbf{0} & & & r_{mn} \end{bmatrix}. \tag{9}$$

In addition, let

$$\pi_{ij}(t) = P_r(Z(t) = j | Z(0) = i), \quad i, j \in T \tag{10}$$

and

$$\pi_j = \lim_{t \to \infty} P_r(Z(t) = j | Z(0) = i), \quad i, j \in T. \tag{11}$$

In other words, $\pi_{ij}(t)$ is the probability that the battery is in state j at time t given that it was initially in state i, and π_j is the limit of $\pi_{ij}(t)$ as t goes to infinity, assuming the CTMC has a stationary distribution. As in the results of Section III, the steady-state probabilities π_j should then satisfy $\mathrm{p_e}\mathcal{Q}_e^{MDP} = 0$ and $\sum_{j \in T} \pi_j = 1$, where $\mathrm{p_e} = [\pi_1 \; \pi_2 \; \ldots \; \pi_{|T|}]$.

TABLE III
NOTATION USED IN SECTION IV

Notation	Description	Value
C	Capacity of the battery	$\mathbb{R}^+$
$X(t)$	Battery level of the sensor node at time t	[0,C]
$Z(t)$	State of battery at time t	$\{1, 2, \cdots, m \times n\}$
h_k	Harvesting rate of energy from surroundings	$[0, h_{max}]$, $k \in (0, m]$
u_l	Energy consumption rate	$[0, u_{max}]$, $l \in (0, n]$
r_i	Rate governing the evolution of the battery at state $i = Z(t)$	$r_{n(k-1)+l} = h_k - u_l$
$\dot{X}_{\text{min}}$	Minimum battery change rate	$-u_{max}$
$\dot{X}_{\text{max}}$	Maximum battery change rate	h_{max}

TABLE IV
NOTATION USED IN SECTION V

Notation	Description	Value
$\mathcal{Q}_e^{MDP}$	Transition rate matrix of CTMC describing transitions between different discretized battery evolution rates	N.A.
D	Diagonal matrix of all possible discretized battery evolution rates	N.A.
F	Cumulative transition probability of battery level	$(0, 1)$
A	Energy availability	[0,1]
$\mathcal{Q}_h^{MDP}$	Transition rate matrix of CTMC describing transitions between different discretized energy harvesting rates	N.A.
$\mathcal{Q}_u^{MDP}$	Transition rate matrix of CTMC describing transitions between different discretized energy consumption rates	N.A.

B. Energy availability

The probability that the node battery of the node contains a non-zero amount of energy is given by the limiting availability, A.

Lemma 3. *The energy availability A is given by*

$$A = 1 - F_1(0) - F_2(0) - \ldots - F_{mn}(0), \qquad (12)$$

where $F_j(x) = \lim_{t\to\infty} F(t, x, j; y, i)$. $F(t, x, j; y, i)$ gives the cumulative transition probability that the battery level $X(t)$ is at most x at time t and that the battery is in state j, given that the battery was originally in state i with battery level y.

Proof. See Appendix C. □

In order to increase A, we have to choose the entries of the grand transition matrix $\mathcal{Q}_e^{MDP}$ appropriately such that the stationary probabilities π_j give us the lowest possible values of $F_j(0)$.

C. Decomposing the CTMC into harvesting and consumption states

Since the harvesting and consumption processes are physically distinct, we can decompose our CTMC into two subchains: one involving the transition between different harvesting rates, and one involving the transition between different consumption rates.

If we assume that the transitions between the harvesting rates take place randomly and independently of the transitions between the consumption rates, for example as in direct solar radiation [36], [37], then we can define a stationary distribution $\mathrm{p_h}$ and a transition matrix $\mathcal{Q}_h^{MDP}$ for the harvesting states, and a stationary distribution $\mathrm{p_u}$ and a transition matrix $\mathcal{Q}_u^{MDP}$ for the consumption states. We can then implement a Markovian scheme to transition between the various consumption rates. Note that $\mathrm{p_h}\mathcal{Q}_h^{MDP} = 0$, $\sum_{k\in\mathcal{Z},k\in(0,m]} \mathrm{p_h}(k) = 1$, $\mathrm{p_u}\mathcal{Q}_u^{MDP} = 0$ and $\sum_{l\in\mathcal{Z},l\in(0,n]} \mathrm{p_u}(l) = 1$. Then, $\mathrm{p_e}$ is the Kronecker product of the two component stationary distributions $\mathrm{p_h} \otimes \mathrm{p_u}$, while $\mathcal{Q}_e^{MDP} \equiv \mathcal{Q}_h^{MDP} \otimes \mathcal{Q}_u^{MDP}$.

Conversely, if we assume that the harvesting rate changes smoothly and periodically, for example as in diffuse solar radiation [38], then we should instead take $\mathcal{Q}_e^{MDP} \equiv \mathcal{Q}_u^{MDP}$ and assume the harvesting rate is sufficiently stationary that we ignore the harvesting transitions in the battery model CTMC. We then measure the harvesting rate h_k regularly and implement the MDP to be discussed in Section VI such that r_i is updated regularly. If the convergence rate of the MDP is faster than the timescale of the variation of the harvesting rate, then this method will be able to reasonably adapt to a changing harvesting rate.

1) Derivation of the harvesting transition matrix (for first assumption): $\mathcal{Q}_h^{MDP}$ and $\mathrm{p_h}$ can be derived from empirical data. For a solar-harvesting sensor node, one could measure the time variation of solar energy over a suitably long period of time, and then fit to the averaged data a CTMC whose statistics match the empirical distribution of solar energy throughout the day [36], [37].

2) Definition of the consumption transition matrix (for both assumptions): $\mathcal{Q}_u^{MDP}$ and $\mathrm{p_u}$ are user-defined inputs. In the MDP formulation to follow, we generate an adaptive transition matrix $\mathcal{Q}_u^{MDP}$ based on the optimization of the quality matrix $Q_m = [Q_{m,ls}]$ to be defined in Section VI-A.

VI. MDP MODEL FOR VARIABLE DUTY CYCLE

With the model described in Sections II and III, we can quantify the performance of our system for a known duty cycle q assuming a sufficiently stationary battery level X such that the QoS metrics obtained can be approximated as instantaneous. Using this information, we can now construct a duty cycle policy that allows our system to respond to environmental variations, such as the sunlight available to a solar-harvesting node, while cognizant of the QoS targets that the system is required to fulfil. The effectiveness of the policy is measured both by the QoS targets, for which a model was provided in Sections II and III, and by the battery level, for which a model was provided in Sections IV and V. In addition, the policy is used to determine a good set of transition rates between the various consumption rates described in Section V-C. The notation used in this section is shown in Table V.

A. MDP for Variable Duty Cycle with Reinforcement Learning

In principle, we could try out every single possibility of q for every possible harvesting rate h_k and consumption rate u_l to determine the best q for each rate of change of the battery level r_i. However, this is likely to be costly in terms of both time and computational resources. By formulating our problem as a Markov Decision Process (MDP) driven by a reinforcement learning algorithm, we could possibly reduce the number of computations, perform them online instead of offline, and make our system adaptive to changing system parameters, such as the instantaneous packet transmission and probing rates.

A MDP is useful to describe a decision making process that allows the system to transit between a set of *states*. MDPs have been used in various works to control duty cycling and channel usage in WSNs [39]–[43]. The decision maker has a set of *actions* that can be chosen to describe the state transitions. Each state transition is associated with an immediate scalar *reward*, which is given to the decision-maker or learner. Here, the goal of the reinforcement learning algorithm is to take actions, transit from one state to another, and maximize the expected sum of the rewards in the long run. To keep track of its rewards, the system maintains a *quality* function for each state-action pair, which is a cumulative measure of the rewards obtained so far, and consults this to take an action (with greedy probability ϵ_t). Thus, by taking actions, obtaining rewards and updating the quality matrix based on this reward, the learner finally converges to a policy which approaches maximum return of rewards.

1) States: We define the set $\mathcal{F}$ of states f_l where $l \in \mathcal{Z}$ and $l \in (0, n]$ such that each state corresponds to a unique consumption rate u_l.
2) Actions: We define the set $\mathcal{G}$ of actions g_s such that each action corresponds to a CTMC transition matrix $\mathcal{Q}_{u,s}^{MDP}$ corresponding to transitions between different discretized energy consumption rates. The action space can be designed such that each $\mathcal{Q}_{u,s}^{MDP}$ has a different stationary distribution. Different actions will then signify different duty cycle probability distributions in the limit of infinite time. For example, we could design an action that constrains the duty cycle to frequently take a low value, and another action that constraints it to frequently take a high value. The size of the square matrix $\mathcal{Q}_{u,s}^{MDP}$ is n. Here, we sample the entire space of possible $\mathcal{Q}_{u}^{MDP}$ to obtain a representative set of transition matrices that span the space and are physically convenient to implement.
3) Rewards: Based on the requirements of the user, be it a need to conserve energy aggressively, to consume energy aggressively, or to maintain a minimum level of QoS statistics by achieving a balance between conservation and consumption, one can define an appropriate reward function to achieve one's objective. Here, we define a reward function that incorporates both QoS statistics and some measure of the amount of energy available to the system to balance the QoS requirements and the energy needs of the system. Since the consumption rate u_l is a function of the duty cycle q, we can use the QoS statistics derived in Section III to derive a reward for each state in the MDP.
   In this work, we examine two different reward functions. The first reward function is an n-dimensional reward column vector with the following constituent entries for the corresponding states l
   $$W(l) = -w_\pi \pi(l) - w_\ell \ell(l)/\ell^*(l) - w_\rho \rho(l) + w_A A, \quad (13)$$
   for some arbitrary weights w_π, w_ℓ, w_ρ and $w_A \in \mathbb{R}^+$, and where $\ell^*(l) = B/(\lambda(u_l) + \lambda_0(u_l))$. This definition of the reward offers a high reward for a low loss probability, low latency, low energy consumption and high energy availability A. Note that since A is dependent on some transition matrix that governs the time evolution of the system, $W(l)$ is not strictly a function of only the system state l, but is a non-stationary function that varies with time.
   The second reward function is a similar column vector with the following constituent entries
   $$W(l) = \begin{cases} w_+ & \pi(l) < \pi_0, \ell(l) < \ell_0, \rho(l) < \rho_0, A \in A_0 = [A_{0,-}, A_{0,+}) \\ w_- & \text{otherwise} \end{cases} \quad (14)$$
   involving the latency and loss thresholds π_0 and ℓ_0 defined earlier in Section III, as well as analogous power consumption and availability thresholds ρ_0 and A_0. In this case, the reward takes one of two discrete values w_+ or w_- instead of a continuous spectrum of values in the earlier example.
   The continuous function (13) enables users to finetune the balance between energy availability and QoS requirements, while the thresholding function (14) enables users who are aware of the thresholds that the system is required to satisfy, such as network engineers, to provide a clear system input.
4) Quality: Last but not least, we associate each state f_l and action g_s with a quality $Q_{m,ls}$.

In Fig. 5, we use a state machine diagram to illustrate the state and action spaces of the MDP.

TABLE V
NOTATION USED IN SECTION VI

Notation	Description	Value
$\mathcal{F}$	Set of states f_l corresponding to a unique u_l	$l \in (0, n]$
$\mathcal{Q}_{u,s}^{MDP}$	Transitions between different discretized energy consumption rates for each action g_s	N.A.
$\mathcal{G}$	Set of actions g_s	$\mathcal{Q}_{u,s}^{MDP}$
$W(l)$	Reward column vector	$\mathcal{R}^+$
A	Energy availability	[0,1]
Q_{m,l_s}	Quality of each state f_l and action g_s	$\mathcal{R}^+$

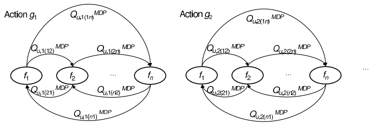

Fig. 5. MDP state and action spaces. $\mathcal{Q}_{u,s(ij)}^{MDP}$ refers to the (i, j)-th entry of the transition rate matrix corresponding to the s-th action.

B. Implementing the MDP

We begin our MDP by selecting a suitable initial guess for the quality matrix $Q_m = [Q_{m,ls}]$, some initial state f_0, and a suitable initial CTMC transition matrix $\mathcal{Q}_{u,a}^{MDP} = \mathcal{Q}_{u,0}^{MDP}$. Then, we evolve our MDP as follows: based on some tuning parameter $0 < \epsilon_t < 1$, we select with probability ϵ_t the action $g_s = g_f \in \mathcal{G}$ with the highest value in the quality matrix Q_m for the corresponding state f_0, or with probability $1 - \epsilon_t$ a random action $g_s = g_r \in \mathcal{G}$. Based on this action, we select the f_0-th row in the transition matrix Q_{u,g_s} corresponding to the action g_s, and replace the f_0-th row in our actual CTMC transition matrix $\mathcal{Q}_{u,a}^{MDP}$ with this row. Then, we evolve the system based on $\mathcal{Q}_{u,a}^{MDP}$. When the system evolves to a new state f_1 based on this transition matrix, the reward associated with the new state $W(f_1)$ is computed using the value of A corresponding to the current matrix $\mathcal{Q}_{u,a}^{MDP}$. Next, the appropriate entry in the quality matrix is computed using the Q-learning method [44]

$$Q_{m,0s,\text{new}} = (1-\mu)Q_{m,0s,\text{old}} + \mu \left(W(f_1) + \gamma \max_{g_{s'}} Q_{m,1s',\text{old}} \right) \quad (15)$$

for some learning rate $0 < \mu < 1$ and some discount factor $\gamma \in [0, 1)$. The next action is then selected using the entries of the updated quality matrix, and the entire process is repeated for the entire time evolution process. The intention is to maximize the following expectation value over all sample paths

$$W_r = \mathbb{E}\left[\int_0^\infty \gamma^t W(f(t))dt\right] \quad (16)$$

where the state of the process at time t is $f(t)$. An optimal solution will attain the maximum possible expected discounted reward W_r. In our adaptive framework, we aim to maximize W_r for the system under consideration by tuning ϵ_t and μ, and choosing an appropriate set of actions $\mathcal{G}$. Under this framework, we believe the CTMC transition matrix $\mathcal{Q}_{u,a}^{MDP}$ increases its optimality over time in the long run and is able to respond to changes in the system parameters.

In Fig. 6, we use a flow diagram to illustrate the reward generation, quality update and decision-making process in the MDP. We also summarize the process in Algorithm 1.

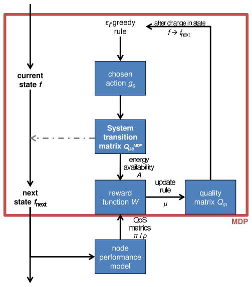

Fig. 6. MDP dynamics. At all times, the system evolves based on knowledge of the current state f and the system transition matrix $Q_{u,a}$. A new action is selected whenever the system undergoes a state transition.

```
Algorithm 1: Procedure for solving MDP
Input: Initial guess for $Q_m$, initial state $f = f_0$, initial
       CTMC transition matrix $\mathcal{Q}_{u,a}^{MDP} = \mathcal{Q}_{u,0}^{MDP}$
Output: Instantaneous (actual) CTMC transition matrix
        $\mathcal{Q}_{u,a}^{MDP}$, Instantaneous state $f$
initialization;
while node is functioning do
    Select action $g_s$;
    With probability $\epsilon_t$, determine if optimal action
    selection is triggered;
    if optimal action selection triggered then
        Select $g_s$ with highest corresponding value in
        $Q_m$ for corresponding state $f$ ;
    else
        Select random $g_s$ ;
    Update $\mathcal{Q}_{u,a}^{MDP}$ based on $g_s$;
    Evolve system in time based on $\mathcal{Q}_{u,a}^{MDP}$ until state $f$
    changes to $f_{\text{next}}$;
    Compute reward $W(f_{\text{next}})$ and update corresponding
    entry in $Q_m$;
    Repeat loop
```

Note that under the assumption of Markovian transitions between harvesting rates, we can choose to either establish a different state space, action space, quality matrix and instantaneous transition matrix for each harvesting rate, or we can choose to evolve a single MDP and simply let it respond to the harvesting rate variation with a time-varying reward (in particular the variation in A). The first option is more rigorous and is likely to provide better convergence, but the second option could be more convenient and less intensive to implement. Under the assumption of a smooth variation of the harvesting rate, we can evolve the MDP as it is and allow it to respond to harvesting rate variations with a time-varying reward, provided the MDP convergence timescale is shorter than the harvesting rate variation timescale.

VII. Simulation Results

In this Section, we present some results obtained using Monte Carlo simulations of a single node involving the simultaneous time evolution of the CTMCs describing the network and battery states of the node, and of the MDP describing the evolution of the duty cycle of the node. We first describe the parameters and the MDP formulation used in the simulation. We then discuss the impact of the reinforcement learning parameters, and evaluate the performance of our algorithm for both the continuous and discrete reward functions highlighted in Section VI.

A. Simulation set-up

The network parameters used in our simulations are described in Table VI. For simplicity, we consider the case where the node in question does not generate its own packets. Also, we first consider the case where the link quality between the nodes in the network is always good (so there is no difference between the Retransmissions and No Retransmissions schemes), and where the energy harvesting rate adopts a constant value of 0.3 energy units per unit time for the duration of the learning. (We relax the link quality and constant harvesting rate assumptions in Sections VII-E and VII-F respectively.) For the chosen set of network parameters, this bounds the possible battery evolution rates between about -0.03 and 0.07 energy units per unit time. Finally, we assign our battery a capacity of 0.05 energy units.

For our MDP, we consider a relatively small state space with 9 states, involving the regularly-spaced duty cycles $\{0.1, 0.2, \cdots, 0.9\}$, as well as a relatively small action space with 5 actions, to make the conclusions we derive from our simulations clearer. The infinitesimal generators corresponding to the five actions are detailed in Appendix D, and have corresponding stationary distributions that are centred around states 1, 3, 5, 7 and 9 respectively. In all trials, we initialize our MDP with a randomly chosen state, an all-zero quality matrix, and a state transition matrix where all inter-state transitions have a rate of 0.1 transitions per unit time, and force the MDP to select an action immediately.

B. Reinforcement learning parameters

We highlight the effects of varying the learning rate μ, the exploitation probability ϵ_t, and the discount factor γ. In particular, we note the trade-off between decreasing the response time of the system and maintaining the stability of the convergence of the learning curves, and make the observation that the reinforcement learning algorithm used in our simulations outperforms a random decision-making scheme.

1) Effects of varying learning rate μ: In Fig. 7, we observe that a higher μ increases the learning ability of the system by decreasing the convergence time, but results in higher-frequency and larger fluctuations in the learned quality values.

2) Effects of varying exploitation probability ϵ_t: In Fig. 8, we again observe that a higher ϵ_t decreases the convergence time of the system at the expense of higher-frequency and larger fluctuations in the learned quality values. In Fig. 9, we observe that as ϵ_t increases, the distribution deviates more strongly from a uniform distribution for the odd-numbered states, which is what we would expect in a system that selects its actions randomly. In addition, as ϵ_t increases, the standard deviations of the probabilities decrease, suggesting convergence towards a desirable stationary distribution. By choosing a non-zero ϵ_t, we obtain a scheme that outperforms a random decision-making policy.

3) Effects of varying discount factor γ: Without a sufficiently large γ, the randomness inherent in a MDP, and especially in the reward function we selected due to the constantly varying nature of A, may impede the learning of the system. In Fig. 10, we observe that only with a sufficiently large γ does effective learning take place in the system.

C. Performance of algorithm: Continuous reward function

The performance of our algorithm depends on our system objectives, as well as the reward function implemented in our MDP. An appropriate choice of the reward function can shift the behaviour of the system. Here, we consider the reward function (13), and look at the effects of varying the weights.

1) Effects of energy availability on system: We expect that in a system that places great emphasis on energy availability, the average duty cycle will be low in order to ensure the battery does not expend all its energy; conversely, in a system that places little emphasis on energy availability, the average duty cycle will then be governed by the QoS metrics, which are likely to push the duty cycle higher to ensure effective transmission. This intuition is validated by the results in Figs. 11 and 13a.

2) Effects of latency on system: We similarly expect that when emphasis on latency is high, the average duty cycle will be high to maintain the QoS standards; conversely, when emphasis on latency is low, the average duty cycle will then be lower to conserve energy and meet the power consumption and energy availability requirements. This intuition is validated by the results in Figs. 12 and 13b.

D. Performance of algorithm: Reward function with thresholding

1) Convergence analysis: Figure 14 plots the quality for a single state and action with respect to different values of power and latency thresholds in order to demonstrate the convergence of the algorithm. When the power threshold is increased with all other thresholds fixed, the magnitude of the quality and the convergence time decrease. When the latency threshold is increased with all other thresholds fixed, the magnitude of the quality and the convergence time increase.

TABLE VI
NETWORK PARAMETERS

Notation	Description (units)	Value
T	Average cycle time (time units)	2
$\lambda_g = \lambda_b$	Average received-packet rate from nearby nodes (per time unit)	0.5
B	FIFO buffer size (packets)	10
$\theta_g = \theta_b$	Intensity of probing (per time unit)	3
$\mathcal{P}_{asleep}$	Power consumption of a node in the asleep state (energy units per time unit)	0.01
$\mathcal{P}_{awake}$	Power consumption of a node in the awake state (energy units per time unit)	0.1
$\mathcal{P}_{probe}$	Power consumption of probing mechanism (energy units per time unit)	0.2
ε_{tx}	Energy consumed to transmit a single data packet (energy units)	0.4

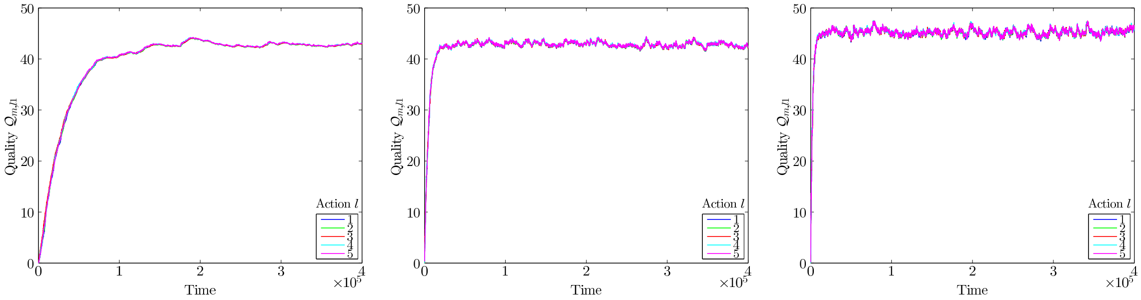

(a) $\mu = 0.1$ (b) $\mu = 0.5$ (c) $\mu = 0.9$

Fig. 7. Graphs of quality $\mathcal{Q}_{m,l1}$ against time for MDP state 1, all actions l and different values of μ for a single trial. Each line represents a different action. Here, $\epsilon_t = 0.5$ and $\gamma = 0.995$. In addition, we use the reward function (13) and set all weights to 1.

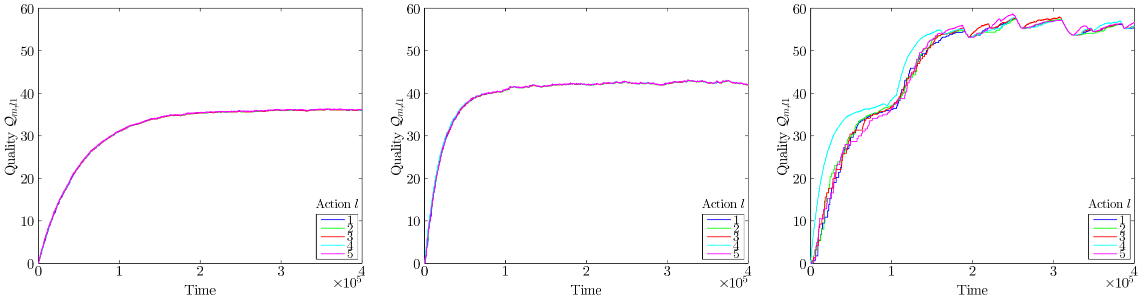

(a) $\epsilon_t = 0.1$ (b) $\epsilon_t = 0.5$ (c) $\epsilon_t = 0.9$

Fig. 8. Graphs of quality $\mathcal{Q}_{m,l1}$ against time for MDP state 1, all actions l and different values of ϵ_t for a single trial. Each line represents a different action. Here, $\mu = 0.1$ and $\gamma = 0.995$. In addition, we use the reward function (13) and set all weights to 1.

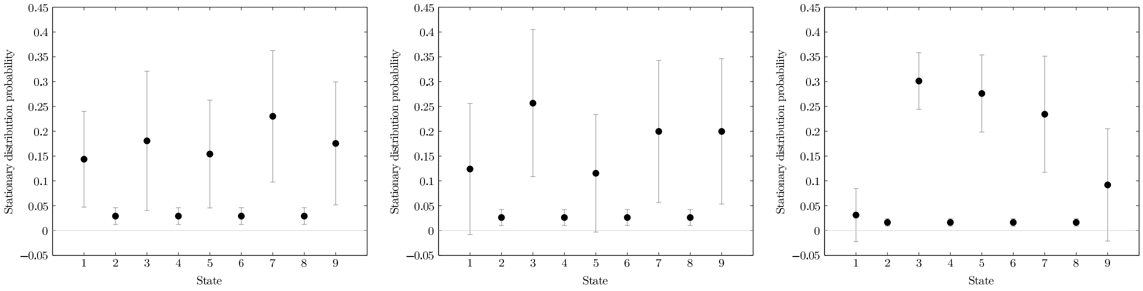

(a) $\epsilon_t = 0.1$ (b) $\epsilon_t = 0.5$ (c) $\epsilon_t = 0.9$

Fig. 9. Stationary distribution based on the transition rate matrix $\mathcal{Q}_{u,a}^{\text{MDP}}$ for the 9 MDP states averaged over 50 trials each for different values of ϵ_t. Here, $\mu = 0.1$ and $\gamma = 0.995$. In addition, we use the reward function (13) and set all weights to 1.

2) Comparison with random approach: Figure 15 shows the effect of various QoS thresholds on the selection of actions, as well as the comparison of the random and ϵ_t-greedy approaches, the latter of which we highlighted in our algorithm above. The three cases of thresholds we consider are: Case I: $\{\rho_0 = 0.3, \ell_0 = 5, \pi_0 = 0.01\}$; Case II:

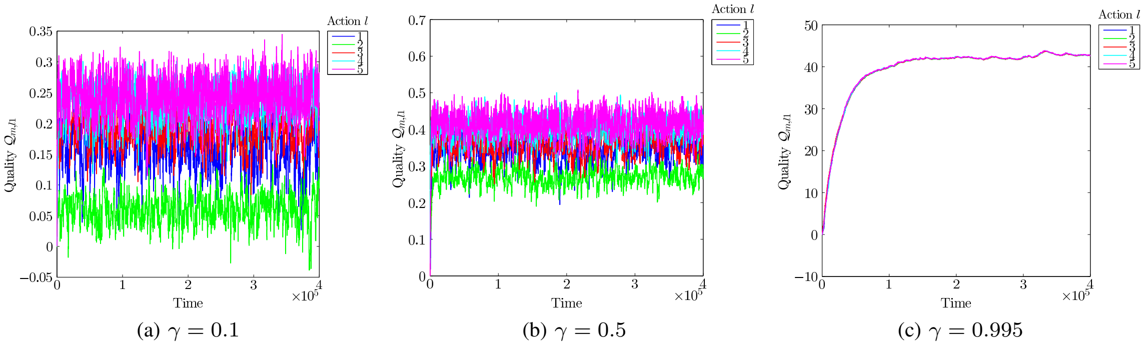

(a) $\gamma = 0.1$

(b) $\gamma = 0.5$

(c) $\gamma = 0.995$

Fig. 10. Graphs of quality $\mathcal{Q}_{m,l1}$ against time for MDP state 1, all actions l and different values of γ for a single trial. Each line represents a different action. Here, $\mu = 0.1$ and $\epsilon_t = 0.5$. In addition, we use the reward function (13) and set all weights to 1.

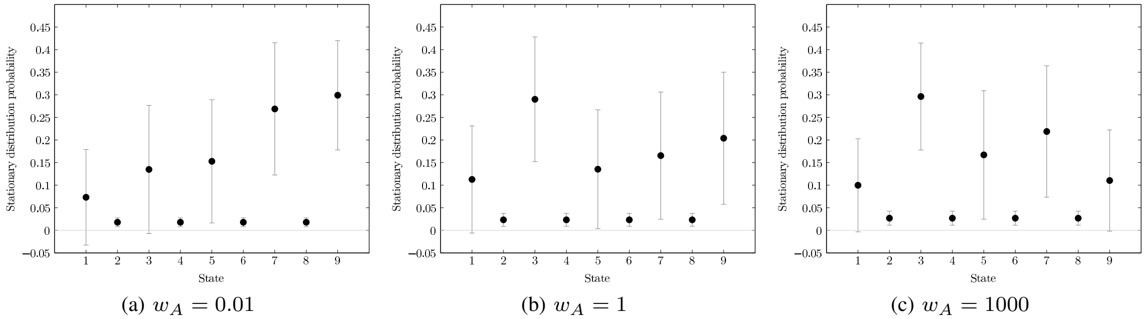

(a) $w_A = 0.01$

(b) $w_A = 1$

(c) $w_A = 1000$

Fig. 11. Stationary distribution based on the transition rate matrix $\mathcal{Q}_{u,a}^{\mathrm{MDP}}$ for the 9 MDP states averaged over 50 trials each for different values of w_A. Here, $\epsilon_t = 0.5$, $\mu = 0.1$ and $\gamma = 0.995$. In addition, we use the reward function (13) and set all other weights to 1.

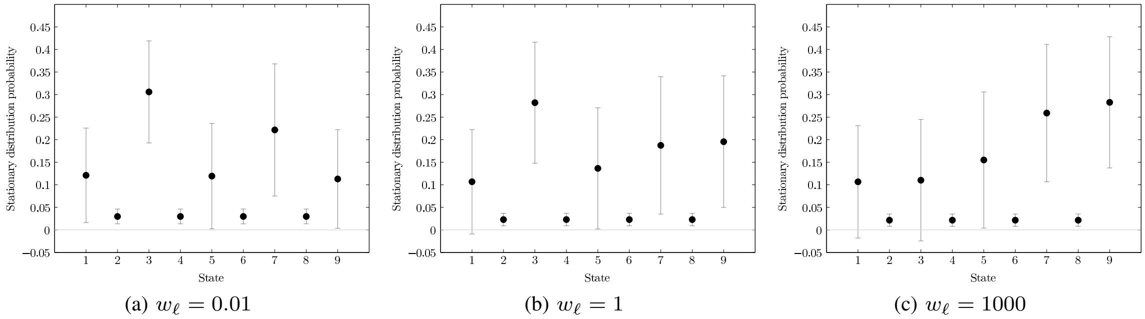

(a) $w_\ell = 0.01$

(b) $w_\ell = 1$

(c) $w_\ell = 1000$

Fig. 12. Stationary distribution based on the transition rate matrix $\mathcal{Q}_{u,a}^{\mathrm{MDP}}$ for the 9 MDP states averaged over 50 trials each for different values of w_ℓ. Here, $\epsilon_t = 0.5$, $\mu = 0.1$ and $\gamma = 0.995$. In addition, we use the reward function (13) and set all other weights to 1.

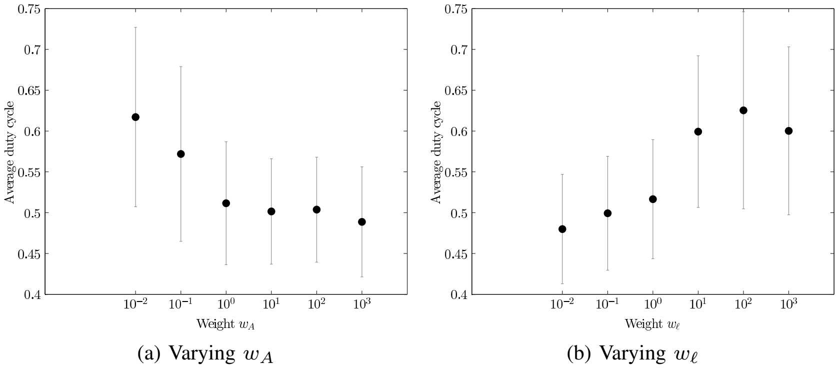

(a) Varying w_A

(b) Varying w_ℓ

Fig. 13. Plot of average duty cycle versus (a) w_A, holding all other weights constant at 1 and (b) w_ℓ, holding all other weights constant at 1, using (13) and averaging over 50 trials for each w_A and w_ℓ respectively. Here, $\epsilon_t = 0.5$, $\mu = 0.1$ and $\gamma = 0.995$.

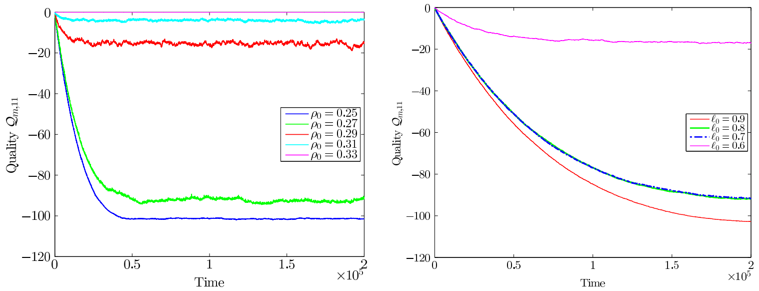

(a) Power

(b) Latency

Fig. 14. Graphs of quality $\mathcal{Q}_{m,11}$ against time for state 1 and action 1, and for different power (ρ_0) and latency (ℓ_0) thresholds. Here, $\epsilon_t = 0.9$ and $\gamma = 0.995$. For (a), $\ell_0 = \pi_0 = A_{0,+} = 1$ and $A_{0,-} = 0$, and for (b), $\rho_0 = \pi_0 = 0.7$, $A_{0,+} = 1$ and $A_{0,-} = 0$.

$\{\rho_0 = 0.32, \ell_0 = 5, \pi_0 = 0.01\}$; Case III: $\{\rho_0 = 0.33, \ell_0 = 0.91, \pi_0 = 4\text{E-}5\}$. Here, we do not consider the effects of energy availability by taking $A_0 = [0, 1)$.

Figure 16 shows the optimal sets of duty cycles for the three cases in order to satisfy the QoS thresholds. In Case I, the corresponding optimal state is 4. In Case II, the corresponding optimal states are 5, 6 and 7. In Case III, the corresponding optimal states are 7, 8 and 9. This agrees with the results shown in Fig. 15 when $\epsilon_t = 0.9$, keeping in mind that our action space tends to direct the system towards the odd-numbered states only. When $\epsilon_t = 0$, the scheme reduces to a random approach where the states are chosen randomly and the stationary probabilities of states 1, 3, 5, 7 and 9 are uniform.

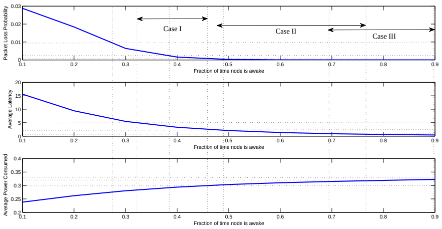

Fig. 16. Optimal sets of duty cycles for each case without considering the energy availability A.

3) Effects of energy availability: As seen in the previous subsection, the QoS thresholds can help to choose a set of optimal duty cycles. However, the energy availability depends on the attainment of equilibrium by the whole system, and the derivation of the optimal set of duty cycles is not as straightforward.

a) Simulation settings: In this section, we modify the learning rate μ to be inversely proportional to the total time spent in the current state [32] in order to handle the variation in the energy availability. In addition, we select a subset of the action space in which the system's steady state probabilities are centred around states 3, 5, 7 and 9 to better illustrate the effects of varying A_0.

b) Convergence analysis: The convergence of the algorithm with the presence of the energy availability term is not as fast with the learning rates used in the previous sections. Hence, we use a learning rate that decreases with total time elapsed in the current state (including past transitions) to speed up convergence. Figure 17 demonstrates the convergence of the learned quality values and the emergence of an optimal action. As seen in Fig. 17a, low values of A_0 result in an action that favours a higher duty cycle and lower energy availability, and vice versa as evident from Figs. 17b and 17c.

c) Analysis of steady state probabilities: Fig. 18a demonstrates that when energy availability is not considered and when all the duty cycles satisfy the given QoS thresholds, the steady state probabilities learned are almost uniform with high standard deviation. This changes in Figs. 18b to 18d, where we see that a low A_0 selects higher duty cycles and a high A_0 selects lower duty cycles on average.

d) Summary: For greater clarity, the results above are summarised in Fig. 19. These graphs demonstrate that an increase in A_0 decreases the average duty cycle and promotes the selection of actions favouring states that correspond to lower duty cycles.

4) Remarks: As we mentioned earlier, the continuous reward function (13) enables finetuning of the balance between energy availability and QoS requirements, while the thresholding reward function (14) enables clear demarcations of the boundaries of the system, provided the intersection of the threshold requirements is physically achievable. Our results demonstrate that the convergence characteristics of both reward mechanisms are comparable and can simultaneously take into consideration short-term QoS requirements and long-term energy availability standards.

E. Varying link quality

We now consider the effects of variable link quality as discussed in the system model in Section II. Here, we use the thresholding reward function (14) analogous to the results in Section VII-D.

1) Convergence analysis: Figure 20 demonstrates the convergence of the learned quality values for different power thresholds when the channel can exist in either the good or bad state, for both the Retransmissions and No Retransmissions schemes.

2) Comparison with random approach: Figure 21 compares the random and ϵ_t-greedy approaches, for the Retransmissions (Case I) and No Retransmissions (Case II) schemes.

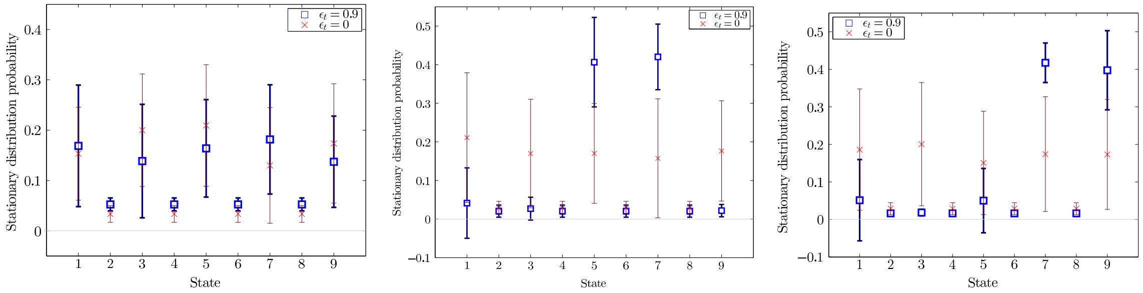

(a) Case I

(b) Case II

(c) Case III

Fig. 15. Comparison of the ϵ_t-greedy approach highlighted in our algorithm above ($\epsilon_t = 0.9$, blue) with a random approach ($\epsilon_t = 0$, red) using the average stationary probability of each state over 20 trials for three different cases of thresholds. The more probable states obtained from our algorithm (in blue) agree well with the optimal duty cycles predicted in Fig. 16.

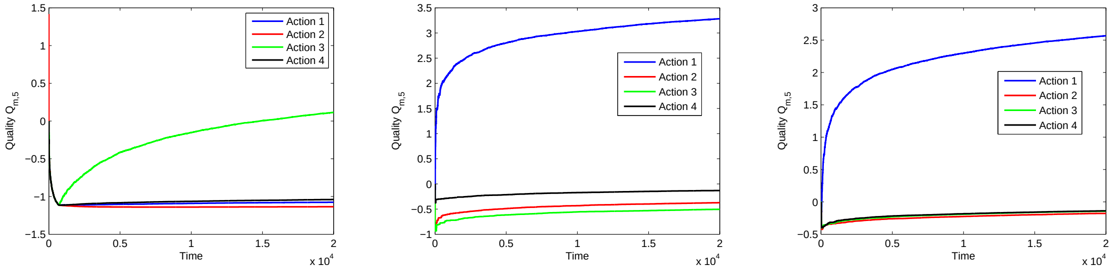

(a) $A_0 \in [0.4, 0.45)$

(b) $A_0 \in [0.5, 0.55)$

(c) $A_0 \in [0.6, 0.65)$

Fig. 17. Graphs of $\mathcal{Q}_{m,5}$ against time for different ranges of A_0. Here, $\pi_0 = 0.02$, $\ell_0 = 9$, $\rho_0 = 0.33$, $\epsilon_t = 0.9$ and $\gamma = 0.995$.

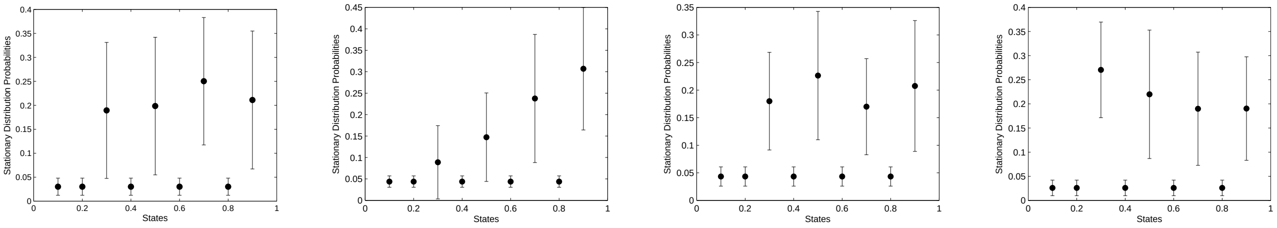

(a) $A_0 \in [0, 1)$

(b) $A_0 \in [0.4, 0.45)$

(c) $A_0 \in [0.5, 0.55)$

(d) $A_0 \in [0.6, 0.65)$

Fig. 18. Graphs of steady state probabilities averaged over 20 trials, for different ranges of A_0. Here, $\pi_0 = 0.02$, $\ell_0 = 9$, $\rho_0 = 0.33$, $\epsilon_t = 0.9$ and $\gamma = 0.995$.

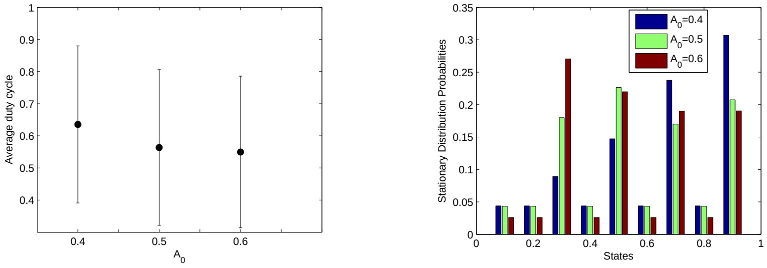

(a) Average duty cycle for different A_0

(b) Average steady state probabilities for different A_0

Fig. 19. Graphs of (a) the duty cycle for different ranges of A_0 plotted against the median of A_0 and (b) the steady state probabilities for different ranges of A_0, both averaged over 20 trials. Here, $\pi_0 = 0.02$, $\ell_0 = 9$, $\rho_0 = 0.33$, $\epsilon_t = 0.9$ and $\gamma = 0.995$.

The thresholds and parameters adopted in these two Cases are identical to those adopted in Fig. 20. The corresponding optimal state for both Cases is 1, and we demonstrate in Fig. 21 that our algorithm is able to learn this optimal condition.

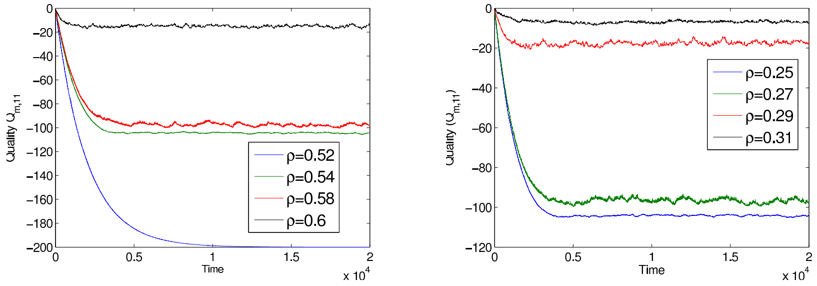

(a) (b)

Fig. 20. Graphs of quality $\mathcal{Q}_{m,11}$ against time for state 1 and action 1, and for different power thresholds (ρ_0) and different re-transmission schemes. Here, $\epsilon_t = 0.9$ and $\gamma = 0.995$, $\ell_0 = \pi_0 = A_{0,+} = 1$ and $A_{0,-} = 0$. (a) Retransmissions scheme: $\lambda_g = \lambda_b = 0.5$. (b) No Retransmissions scheme: $\lambda_g = 0.5, \lambda_b = 0.3$.

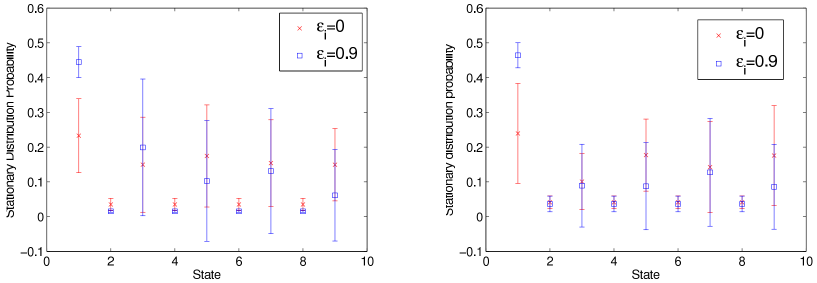

(a) Case I (Retransmissions) (b) Case II (No Retransmissions)

Fig. 21. Comparison of the ϵ_t-greedy approach in our algorithm ($\epsilon_t = 0.9$) with a random approach ($\epsilon_t = 0$) using the average stationary probability of each state over 10 trials for two different cases of thresholds. The values of λ_g and λ_b are identical to those in Fig. 20.

F. *Varying harvesting rate*

We now consider the effects of variable harvesting rate to simulate environmental fluctuations. Here, we again use the thresholding reward function (14) and the same simulation settings as Section VII-D3a.

1) Simulation setup: In the simulations to be described, we used 4 different values of the harvesting rate $h_{\text{arr}} = [0.2,\ 0.2875,\ 0.3,\ 0.4]$ where the lowest rate corresponds to zero energy availability ($A = 0$) and the largest rate corresponds to maximum energy availability ($A = 1$). In addition, we define the harvesting rate to vary in a cyclical manner such that h_{arr} is uniformly distributed over time.

2) Simulation Results:

a) Reward histogram: The reward histograms in Fig. 22 summarize the frequency of the rewards obtained after a single trial (excluding transient variations) for two different sets of A_0. In both cases, a reward of $+1$ is obtained around 67% of the time even under a varying harvesting rate. Under these conditions, the instantaneous network parameters satisfy the predefined thresholds.

b) Convergence of the quality matrix: As similar to Section VII-D3a, we used a time-varying learning rate to handle the changing environment. As demonstrated in Fig. 23, this has proven to be effective: when $A_0 = [0.6, 1]$, the preferred action takes the system from state 5 to state 3 to ensure sufficient energy availability, and when $A_0 = [0.4, 1]$, the preferred action takes the system state 5 to state 7 as the threshold for energy availability relaxes.

c) Comparison of the average steady state probabilities: From Fig. 24, it is evident that when $A_0 = [0.6, 1]$, the lower duty cycle states are preferred, in contrast to the case when $A_0 = [0.4, 1]$, where higher duty cycle states are preferred. Thus, our algorithm is cognizant of the requirements in our system even under varying environmental conditions.

VIII. Conclusion

In this paper, we develop an adaptive duty cycling scheme in wireless sensor networks that takes into account both the energy supply dynamics and application-level QoS requirements at the same time. Continuous Time Markov Chain (CTMC) models are used to derive analytical expressions for these QoS metrics - such as latency, loss probability and average energy consumption - as well as for the energy availability of the system, which offers a probabilistic measure of the ability of the battery to maintain a non-zero energy level on average. We then establish a reward framework that allows the network to tune the relative importance of the energy availability and the QoS requirements, and we perform numerical simulations to verify our model. We implement a reinforcement learning algorithm that converges to a desirable solution quickly and with lower computational complexity than a completely optimal algorithm, and show that our adaptive scheme performs better than a random scheme. With the quick convergence of our algorithm, we enable the possibility of the system adapting to changes in the energy supply dynamics or the network transmission statistics that take place at timescales larger than the convergence time of the learning curve. We intend to extend this work by looking at update rules and threshold functions that enhance the decision-making ability of the system, and hopefully further increase the responsiveness of the system to unexpected externalities.

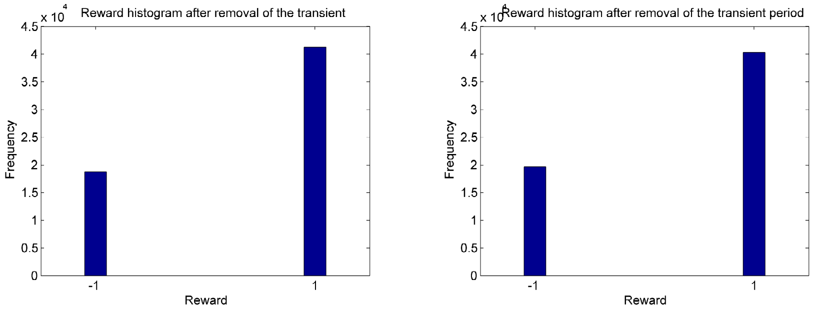

(a) Case I

(b) Case II

Fig. 22. Histogram of rewards following the transient period for a single trial for two different sets of energy availability thresholds A_0. In Case I, $A_0 = [0.4, 1]$, and in Case II, $A_0 = [0.6, 1]$.

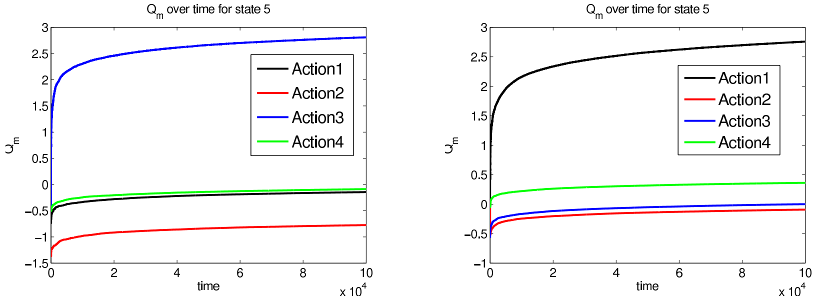

(a) Case I

(b) Case II

Fig. 23. Quality value $\mathcal{Q}_{m,5s}$ for the fifth state and various actions for a single trial for two different sets of energy availability thresholds A_0. In Case I, $A_0 = [0.4, 1]$, and in Case II, $A_0 = [0.6, 1]$.

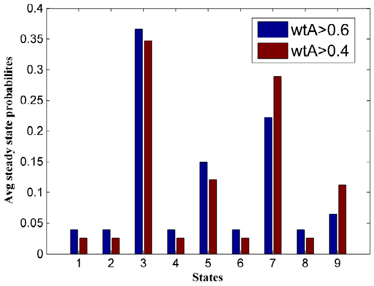

Fig. 24. Steady state probabilities for two different sets of energy availability thresholds A_0 over an average of 5 trials. In Case I (red), $A_0 = [0.4, 1]$, and in Case II (blue), $A_0 = [0.6, 1]$.

Appendix A
Proof of Lemma 1 (Appendix)

We define the QoS metrics, as follows:

1) *Loss probability* $\pi(q)$: The loss probability $\pi(q)$ describes the event that there is incoming traffic (either from the node itself or its neighbors), when the buffer is already full, for a given duty cycle q. This is given by $\pi(q) = P_r(b = B|d_0 = 0, d_n = 1) + P_r(b = B|d_0 = 1, d_n = 0)$.
2) *Latency* $\ell(q)$: The latency ℓ is given by Little's Law $\ell = \frac{\bar{b}}{\lambda_e}$, where $\bar{b}$ is the average number of packets in the buffer, and λ_e is the effective packet arrival rate at the node

$$\ell(q) = \mathbb{E}[\frac{b}{\lambda + \lambda_0}]. \tag{17}$$

3) *Average power consumption* $\rho(q)$: The average power consumption ρ of a node v_j is the sum of the power expended for the probing mechanism, packet transmissions, and other normal operations in each node state

$$\rho(q) = \mathcal{P}_{asleep}P_r(N_j = 0) \\ + (\mathcal{P}_{awake} + \mathcal{P}_{probe})P_r(N_j = 1) + (\lambda + \lambda_0)\mathcal{E}_{tx}. \tag{18}$$

We derive these quantities in (5) to (6) for the two transmission schemes $\mathcal{X}_r$ (Retransmissions) and $\mathcal{X}_n$ (No Retransmissions) as described in Section II.

To calculate these QoS metrics, we solve the steady state probabilities of the CTMC system, i.e. the long term probabilities of being in each state of the state space. The steady-state probability of an arbitrary state $s_k \in \mathcal{S}$ is given by $p_k = \lim_{t\to\infty} P_r(\mathcal{S}(t) = s_k)$. We let $\mathrm{p} = [p_1 \; p_2 \; ... \; p_{|\mathcal{S}|}]$. The steady state probabilities can then be obtained by solving $\mathrm{p}\mathcal{Q} = \mathbf{0}$ and $\sum_{s_k\in\mathcal{S}} p_k = 1$, where $\mathcal{Q}$ is the transition matrix of the CTMC.

Appendix B
Proof of Lemma 2 (Appendix)

The procedure for the calculation of the QoS metrics for the No Retransmissions scheme is identical to the procedure for the calculation of the metrics for the Retransmissions scheme, except that care has to be taken to distinguish between the different packet transmission rates for the good and bad link quality states. In addition, the power consumption for the No Retransmissions scheme is lower than that for the Retransmissions scheme exactly by the amount of energy required to retransmit the packets.

Appendix C
Proof of Lemma 3 (Appendix)

A. Transient behaviour of battery

Let $F(t, x, j; y, i) = P_r(X(t) \leq x, Z(t) = j|X(0) = y, Z(0) = i)$. $F(t, x, j; y, i)$ gives the cumulative transition probability that the battery level $X(t)$ is at most x at time t and that the battery is in state j, given that the battery was originally in state i with battery level y. It can be shown that the cumulative transition probability mn-by-mn matrix $F(t, x; y) = [f_{ij}]$ satisfies the equations

$$\frac{\partial F(t, x; y)}{\partial t} + \frac{\partial F(t, x; y)}{\partial x} D = F(t, x; y)\mathcal{Q}_e^{MDP} \tag{19}$$

for each $x \in [0, C]$ and $y \in [0, C]$, with boundary conditions

$$\begin{aligned} F(t, 0, j; y, i) &= 0, && \text{if } r_j > 0, \\ F(t, C, j; y, i) &= \pi_{ij}(t), && \text{if } r_j < 0. \end{aligned} \tag{20}$$

B. Steady-state behaviour of battery

As t goes to infinity, the limits of (19) and (20) become, for the mn-dimensional row vector $F(x)$ with entries $F(x, j)$,

$$\frac{dF(x)}{dx} D = F(x)\mathcal{Q}_e^{MDP} \tag{21}$$

for each $x \in [0, C]$, with boundary conditions

$$\begin{aligned} F(0, j) &= 0 && \text{if } r_j > 0, \\ F(C, j) &= \pi_j && \text{if } r_j < 0. \end{aligned} \tag{22}$$

We see that

$$F' = F(\mathcal{Q}_e^{MDP} D^{-1}), \tag{23}$$

which leads us to guess the solutions $F(x) = e^{\lambda x}\phi$ where λ is a scalar and ϕ is an mn-dimensional row vector. It can be shown that the general solution to (23) is given by $F(x) = \sum_{i \in T} a_i e^{\lambda_i x} \phi_i$, where λ_i are the generalized eigenvalues and ϕ_i the generalized eigenvectors of the equation

$$\phi_i(\lambda_i D - \mathcal{Q}_e^{MDP}) = 0 \tag{24}$$

or

$$((\mathcal{Q}^{MDP})_e^T - \lambda_i D^T)\phi_i^T = 0. \tag{25}$$

In other words, λ_i and ϕ_i^T are the eigenvectors of $(D^{-1})^T(\mathcal{Q}^{MDP})_e^T = ((\mathcal{Q}^{MDP})_e D^{-1})^T$.

The coefficients a_i are given by the solutions to

$$\begin{aligned} \sum_{i \in T} a_i \phi_i(j) &= 0 && \text{if } j \in T^+, \\ \sum_{i \in T} a_i \phi_i(j) e^{\lambda_i C} &= \pi_j && \text{if } j \in T^-, \end{aligned} \tag{26}$$

where T^+ and T^- contain the elements of T where the corresponding rate r_j is positive and negative respectively. Note that keeping all else constant, a higher C results in lower a_i and thus a larger A.

Appendix D
Action Space of MDP Used for Simulations (Appendix)

The infinitesimal generators corresponding to the five actions are such that they encourage the system to transition to states 1, 3, 5, 7 and 9 respectively. An action that transitions the system to some state i has an infinitesimal generator where state i has a transition rate of 0.1 to all other states, and all other states have transition rates of 0.9 to state i and 0.1 to all other states. For example, for action 1, the infinitesimal generator is

$$\mathcal{Q}_{u,1}^{MDP} = \begin{bmatrix} -0.8 & 0.1 & 0.1 & 0.1 & 0.1 & 0.1 & 0.1 & 0.1 & 0.1 \\ 0.9 & -1 & 0.0143 & 0.0143 & 0.0143 & 0.0143 & 0.0143 & 0.0143 & 0.0143 \\ 0.9 & 0.0143 & -1 & 0.0143 & 0.0143 & 0.0143 & 0.0143 & 0.0143 & 0.0143 \\ 0.9 & 0.0143 & 0.0143 & -1 & 0.0143 & 0.0143 & 0.0143 & 0.0143 & 0.0143 \\ 0.9 & 0.0143 & 0.0143 & 0.0143 & -1 & 0.0143 & 0.0143 & 0.0143 & 0.0143 \\ 0.9 & 0.0143 & 0.0143 & 0.0143 & 0.0143 & -1 & 0.0143 & 0.0143 & 0.0143 \\ 0.9 & 0.0143 & 0.0143 & 0.0143 & 0.0143 & 0.0143 & -1 & 0.0143 & 0.0143 \\ 0.9 & 0.0143 & 0.0143 & 0.0143 & 0.0143 & 0.0143 & 0.0143 & -1 & 0.0143 \\ 0.9 & 0.0143 & 0.0143 & 0.0143 & 0.0143 & 0.0143 & 0.0143 & 0.0143 & -1 \end{bmatrix}. \tag{27}$$

References

[1] A. Kottas, Z. Wang, and A. Rodrguez, "Spatial modeling for risk assessment of extreme values from environmental time series: a bayesian nonparametric approach," *Environmetrics*, vol. 23, no. 8, 2012.

[2] C. Fonseca and H. Ferreira, "Stability and contagion measures for spatial extreme value analyses," *arXiv preprint arXiv:1206.1228*, 2012.

[3] J. P. French and S. R. Sain, "Spatio-temporal exceedance locations and confidence regions," *Annals of Applied Statistics. Prepress*, 2013.

[4] I. Akyildiz, W. Su, Y. Sankarasubramaniam, and E. Cayirci, "Wireless sensor networks: a survey," *Computer networks*, vol. 38, no. 4, pp. 393–422, 2002.

[5] W. K. Seah, Z. A. Eu, and H.-P. Tan, "Wireless sensor networks powered by ambient energy harvesting (wsn-heap)-survey and challenges," in *1st International Conference on Wireless Communication, Vehicular Technology, Information Theory and Aerospace & Electronic Systems Technology.* IEEE, 2009, pp. 1–5.

[6] V. Raghunathan, A. Kansal, J. Hsu, J. Friedman, and M. Srivastava, "Design considerations for solar energy harvesting wireless embedded systems," *Fourth International Symposium on Information Processing in Sensor Networks*, pp. 457 – 462, April 2005.

[7] M. Gorlatova, P. Kinget, I. Kymissis, D. Rubenstein, X. Wang, and G. Zussman, "Challenge: ultra-low-power energy-harvesting active networked tags (enhants)," *Proceedings of the 15th annual international conference on Mobile computing and networking*, pp. 253–260, 2009.

[8] C. Bergonzini, D. Brunelli, and L. Benini, "Algorithms for harvested energy prediction in batteryless wireless sensor networks," *3rd International Workshop on Advances in sensors and Interfaces*, pp. 144 –149, June 2009.

[9] D. Hasenfratz, A. Meier, C. Moser, J.-J. Chen, and L. Thiele, "Analysis, comparison, and optimization of routing protocols for energy harvesting wireless sensor networks," *IEEE International Conference on Sensor Networks, Ubiquitous, and Trustworthy Computing (SUTC)*, pp. 19 –26, June 2010.

[10] S. Sudevalayam and P. Kulkarni, "Energy harvesting sensor nodes: Survey and implications," *IEEE Communications Surveys Tutorials*, no. 99, pp. 1–19, 2010.

[11] A. Kansal, J. Hsu, S. Zahedi, and M. B. Srivastava, "Power management in energy harvesting sensor networks," *ACM Trans. Emb. Comput. Sys.*, vol. 6, pp. 1–38, Sep. 2007.

[12] J. Hsu, S. Zahedi, A. Kansal, M. Srivastava, and V. Raghunathan, "Adaptive duty cycling for energy harvesting systems," in *Proceedings of the 2006 international symposium on low power electronics and design.* ACM, 2006, pp. 180–185.

[13] C. Vigorito, D. Ganesan, and A. Barto, "Adaptive control of duty cycling in energy-harvesting wireless sensor networks," in *Proc. IEEE SECON*, 2007.

[14] Y. Gu, T. Zhu, and T. He, "Esc: Energy synchronized communication in sustainable sensor networks," in *Proc. IEEE ICNP*, 2009.

[15] T. Zhu, Z. Zhong, Y. Gu, T. He, and Z.-L. Zhang, "Leakage-aware energy synchronization for wireless sensor networks," in *Proc. ACM MobiSys*, 2009.

[16] V. Sharma, U. Mukherji, V. Joseph, and S. Gupta, "Optimal energy management policies for energy harvesting sensor nodes," *IEEE Transactions on Wireless Communications*, vol. 9, no. 4, pp. 1326–1336, 2010.

[17] C. Moser, J.-J. Chen, and L. Thiele, "An energy management framework for energy harvesting embedded systems," *ACM Journal on Emerging Technologies in Computing Systems (JETC)*, vol. 6, no. 2, p. 7, 2010.

[18] A. Sinha and A. Chandrakasan, "Dynamic power management in wireless sensor networks," *Design & Test of Computers, IEEE*, vol. 18, no. 2, pp. 62–74, 2001.

[19] M. Gorlatova, A. Wallwater, and G. Zussman, "Networking low-power energy harvesting devices: Measurements and algorithms," *IEEE Transactions on Mobile Computing*, vol. 12, no. 9, pp. 1853–1865, Sept 2013.

[20] K. Sohrabi, J. Gao, V. Ailawadhi, and G. J. Pottie, "Protocols for self-organization of a wireless sensor network," *IEEE personal communications*, vol. 7, no. 5, pp. 16–27, 2000.

[21] W. B. Heinzelman, A. L. Murphy, H. S. Carvalho, and M. A. Perillo, "Middleware to support sensor network applications," *IEEE Network*, vol. 18, no. 1, pp. 6–14, 2004.

[22] J. Yick, B. Mukherjee, and D. Ghosal, "Wireless sensor network survey," *Computer networks*, vol. 52, no. 12, pp. 2292–2330, 2008.

[23] J. Lei, R. Yates, and L. Greenstein, "A generic model for optimizing single-hop transmission policy of replenishable sensors," *Wireless Communications, IEEE Transactions on*, vol. 8, no. 2, pp. 547–551, 2009.

[24] A. Seyedi and B. Sikdar, "Energy efficient transmission strategies for body sensor networks with energy harvesting," *Communications, IEEE Transactions on*, vol. 58, no. 7, pp. 2116–2126, 2010.

[25] H. Li, N. Jaggi, and B. Sikdar, "Relay scheduling for cooperative communications in sensor networks with energy harvesting," *IEEE Transactions on Wireless Communications*, vol. 10, no. 9, pp. 2918–2928, September 2011.

[26] A. Sultan, "Sensing and transmit energy optimization for an energy harvesting cognitive radio," *Wireless Communications Letters, IEEE*, vol. 1, no. 5, pp. 500–503, 2012.

[27] P. Blasco, D. Gunduz, and M. Dohler, "A learning theoretic approach to energy harvesting communication system optimization," *IEEE Transactions on Wireless Communications*, vol. 12, no. 4, pp. 1872–1882, April 2013.

[28] R. Chan, P. Zhang, W. Zhang, I. Nevat, A. Valera, H.-X. Tan, and N. Gautam, "Adaptive duty cycling in sensor networks via continuous time markov chain modeling," *Accepted by ICC 2015*, June 2015.

[29] V. G. Kulkarni, "Fluid models for single buffer systems," *Frontiers in queueing: Models and applications in science and engineering*, pp. 321–338, 1997.

[30] G. L. Jones, P. G. Harrison, U. Harder, and T. Field, "Fluid queue models of battery life," in *2011 IEEE 19th International Symposium on Modeling, Analysis & Simulation of Computer and Telecommunication Systems (MASCOTS).* IEEE, 2011, pp. 278–285.

[31] N. Gautam and A. Mohapatra, "Efficiently operating wireless nodes powered by renewable energy sources," *IEEE Journal on Selected Areas in Communications (To appear)*, 2015.

[32] A. G. Barto, *Reinforcement learning: An introduction.* MIT press, 1998.

[33] L. P. Kaelbling, M. L. Littman, and A. W. Moore, "Reinforcement learning: A survey," *Journal of artificial intelligence research*, pp. 237–285, 1996.

[34] E. N. Gilbert, "Capacity of a burst-noise channel," *Bell System Technical Journal*, vol. 39, no. 5, 1960.

[35] E. O. Elliot, "Estimates of error rates for codes on burst-noise channels," *Bell System Technical Journal*, vol. 42, no. 5, 1963.

[36] P. Poggi, G. Notton, M. Muselli, and A. Louche, "Stochastic study of hourly total solar radiation in corsica using a markov model," *International Journal of Climatology*, vol. 20, no. 14, pp. 1843–1860, 2000.

[37] O. Kwon, Y.-J. Yoon, S. K. Moon, H.-J. Choi, and J. H. Shim, "Estimation of singapores hourly solar radiation using hybrid-markov transition matrices method," *International Journal of Precision Engineering and Manufacturing*, vol. 14, no. 2, pp. 323–327, 2013.

[38] R. Jayaraman and D. L. Maskell, "Temporal and spatial variations of the solar radiation observed in singapore," *Energy Procedia*, vol. 25, pp. 108–117, 2012.

[39] Z. Liu and I. Elhanany, "Rl-mac: A qos-aware reinforcement learning based mac protocol for wireless sensor networks," in *Proceedings of the 2006 IEEE International Conference on Networking, Sensing and Control.* IEEE, 2006, pp. 768–773.

[40] ——, "Rl-mac: a reinforcement learning based mac protocol for wireless sensor networks," *International Journal of Sensor Networks*, vol. 1, no. 3, pp. 117–124, 2006.

[41] G. Ghidini and S. K. Das, "An energy-efficient markov chain-based randomized duty cycling scheme for wireless sensor networks," in *Distributed Computing Systems (ICDCS), 2011 31st International Conference on.* IEEE, 2011, pp. 67–76.

[42] M. Bkassiny, S. K. Jayaweera, and K. A. Avery, "Distributed reinforcement learning based mac protocols for autonomous cognitive secondary users," in *Wireless and Optical Communications Conference (WOCC), 2011 20th Annual.* IEEE, 2011, pp. 1–6.

[43] G. Ghidini and S. K. Das, "Energy-efficient markov chain-based duty cycling schemes for greener wireless sensor networks," *ACM Journal on Emerging Technologies in Computing Systems (JETC)*, vol. 8, no. 4, p. 29, 2012.

[44] C. J. Watkins and P. Dayan, "Q-learning," *Machine learning*, vol. 8, no. 3-4, pp. 279–292, 1992.